Wiley
Stem Cells International
Volume 2025, Article ID 4700736, 15 pages
https://doi.org/10.1155/sci/4700736

WILEY

Research Article

Modeling Thoracic Aortic Dissection Using Patient-Specific iPSCs Reveals VSMC Dysfunction and Extracellular Matrix Dysregulation

Peifeng Jin,[1] Yubin Xu,[2] Sixian Wang,[2] Lu Ding,[2] Yuhao Chen,[2] Miqi Zhou,[2] Xiufang Chen,[3] Xiaofang Fan,[2] Yongsheng Gong,[2] Ming Li,[4] and Yongyu Wang [2,4]

[1]*Department of Cardiac Surgery, The First Affiliated Hospital of Wenzhou Medical University, Wenzhou 325000, Zhejiang, China*
[2]*Institute of Hypoxia Medicine, School of Basic Medical Sciences, Wenzhou Medical University, Wenzhou 325015, Zhejiang, China*
[3]*Department of Biochemistry and Molecular Biology, School of Basic Medical Sciences, Wenzhou Medical University, Wenzhou 325015, Zhejiang, China*
[4]*Cardiac Regeneration Research Institute, School of Basic Medical Sciences, Wenzhou Medical University, Wenzhou 325015, Zhejiang, China*

Correspondence should be addressed to Yongyu Wang; yywangut@163.com

Received 31 December 2024; Revised 5 September 2025; Accepted 21 November 2025

Academic Editor: Ludovic Zimmerlin

Copyright © 2025 Peifeng Jin et al. Stem Cells International published by John Wiley & Sons Ltd. This is an open access article under the terms of the Creative Commons Attribution License, which permits use, distribution and reproduction in any medium, provided the original work is properly cited.

Thoracic aortic dissection (TAD) is a life-threatening condition characterized by medial degeneration and vascular smooth muscle cell (VSMC) dysfunction, with no effective medical therapy currently available. The underlying pathological mechanisms of TAD remain incompletely understood. In this study, we used a nonintegrated episomal vector-based reprograming system to generate induced pluripotent stem cells (iPSCs) from TAD patients and healthy controls. Both TAD and normal iPSCs expressed key pluripotency markers and were capable of differentiating into the three germ layers in vitro. These iPSCs were differentiated into vascular smooth muscle cells (VSMCs) through a mesodermal intermediate for disease modeling. VSMCs derived from both TAD and normal iPSCs expressed smooth muscle α-actin (α-SMA), calponin (CNN), and SM22α. However, TAD–iPSC-derived VSMCs exhibited significantly reduced contraction in response to carbachol stimulation compared to their normal counterparts. Whole-exome sequencing identified a mutation in the COL4A2 gene (c.392G > T, p. R131M) in TAD–iPSCs. This mutation was associated with reduced collagen IV expression and increased expression of collagen I and III in TAD-VSMCs, both with and without TGF-β stimulation. Furthermore, noncanonical TGF-β signaling was hyperactivated in TAD-VSMCs, accompanied by elevated MMP9 expression. This patient-specific iPSC model reveals key dysfunctions in VSMC contractility, extracellular matrix (ECM) protein expression, and dysregulated TGF-β signaling, which may contribute to TAD pathogenesis. Our findings provide new insights into the molecular mechanisms driving TAD and offer a platform for future therapeutic development.

Keywords: collagen IV; disease modeling; iPSCs; thoracic Aortic dissection; VSMCs

1. Introduction

Thoracic aortic dissection (TAD) is an aggressive and life-threatening vascular disease with high mortality [1–3], affecting ~3–4 cases per 100,000 annually [4]. This condition is characterized by a tear in the aortic wall, leading to the separation of the layers of the aorta, which can result in severe complications such as rupture or organ damage. The pathogenesis of TAD is complex and multifactorial. Major risk factors include hypertension, dyslipidemia, aging, and genetic predisposition. Genetic analysis has revealed that over 20% of individuals with TAD or thoracic aortic aneurysm (TAA)—defined as a dilation of the thoracic aorta to a diameter at least 1.5 times greater than normal at a given

aortic level—possess single-gene mutations [5]. To date, more than 30 genes associated with TAD and TAA have been identified, emphasizing the genetic component of this disease [6]. Current understanding of TAD pathogenesis is limited, and no effective medical therapies are available. The standard treatment involves surgical intervention, which carries significant risks and limitations [7]. The lack of effective pharmacological treatments underscores the urgent need for novel therapeutic strategies and a deeper understanding of the disease mechanisms. Although extracellular matrix (ECM) degradation and inflammation have been suggested as the key features of TAD, the precise mechanisms still need to be characterized [2, 8].

The aorta wall is composed of three layers; the tunica intima, tunica media, and tunica adventitia. The media of the aortic wall consists of smooth muscle cells and ECM, which includes elastic fibers, collagen, proteoglycans, glycosaminoglycans, and various adhesive proteins. Maintaining ECM homeostasis is critical for normal aortic function, and dysregulation of ECM is associated with TAD, characterized by medial degeneration. Collagen is a crucial component of the ECM, essential for maintaining the structure and function of the aorta. Type I and III collagen are the most abundant collagen present in the aortic wall and show increased expression and deposited in TAD. Mutations in the *COL3A1* gene are linked to vascular-type Ehlers–Danlos syndrome, leading to abnormal collagen fibrillogenesis and TAD formation [9]. Additionally, mice with *col1a1* mutations also exhibit age-dependent onset of aortic dissection [10]. Conversely, the type IV collagen, a basement membrane-specific collagen, is expected to have decreased expression in TAD [11]. Although mutations in collagen-encoding genes are closely associated with aortic dissection, the underlying mechanisms remain unclear.

Vascular smooth muscle cells (VSMCs) play an essential role in the pathogenesis of aortic dissections [12]. The primary function of VSMCs in blood vessels is to regulate blood pressure and blood flow distribution. VSMCs can undergo phenotypic switching in response to various pathological conditions, such as atherosclerosis, hypertension, and restenosis. In these cases, contractile SMCs switch to synthetic phenotype, characterized by reduced expression of contractile and cytoskeletal proteins, increased proliferation and migration, and overproduction of components involved in aortic wall remodeling, such as matrix metalloproteinases (MMPs) [13]. The loss of the contractile phenotype of VSMCs is recognized as an early event in TAA [14]. However, whether the phenotypic switching of VSMCs mediates collagen mutation-induced aortic dissection remains unclear.

Recent advances in stem cell technology offer promising avenues for disease modeling and therapeutic development. Induced pluripotent stem cells (iPSCs), which are generated by reprograming somatic cells, have the potential to differentiate into various cell types and provide valuable insights into disease mechanisms at the cellular level. iPSCs can be derived from patients with specific genetic conditions, allowing the creation of patient-specific disease models [15]. These models can be used to study the molecular and cellular bases of various diseases, including cardiovascular disease, and in testing potential therapeutic agents [16, 17]. For instance, Granata et al. successfully used Marfan syndrome (MFS)-iPSC to model the key mechanism of smooth muscle cell death in MFS [18]. Similarly, generation of patient-specific iPSC from TAD patients in this study may serve as a new powerful tool to study the molecular mechanisms of TAD in vitro.

In this study, we employed a non-integrated episomal vector-based reprograming system to generate iPSCs from TAD patients and healthy controls [19]. Our aim was to investigate the cellular and molecular mechanisms underlying TAD using these patient-specific iPSCs. By comparing the properties and behaviors of TAD patient-derived iPSCs with those from healthy individuals, we observed that TAD–iPSC-derived VSMCs exhibited dysfunction, including reduced contractile response and elevated cell proliferation rates. Additionally, a COL4A2 mutation was identified in TAD–iPSC, which showed decreased expression of type IV collagen and increased expression of type I and III collagen. Furthermore, we found that the ERK-mediated noncanonical TGF-β pathway was activated while the canonical TGF-β-Smad pathway was repressed, indicating that TGF-β is a key pathway and a potential therapeutic target involved in TAD pathogenesis.

2. Materials and Methods

2.1. Isolation and Culture of Primary Aortic SMCs. The aortic tissues from TAD were obtained from the Department of Cardiothoracic Surgery at the First Affiliated Hospital of Wenzhou Medical University. The aortic specimens were washed twice with HBSS (invitrogen). The endothelial layer and the tunica adventitia were removed, and the tunica media was cut into pieces of about 1 mm^3 explants and were placed in a flask for overnight culture with a small amount of Dulbecco's Modified Eagle's Medium (DMEM) with 10% fetal bovine serum and 1% penicillin/streptomycin at 37°C with 5% CO_2 as a previous report [20]. The medium was replenished to cover the explants on the next day. The medium was changed every 3–4 days till the outgrown cell monolayer reached 90% of confluence (normally taking 2–3 weeks). The primary cells were then passaged for iPSC reprograming.

2.2. Generation of Human iPSCs. The nonintegrative iPSCs were generated by nucleofecting TAD-VSMC or BJ cells (normal skin fibroblasts) with episomal vectors (total 3 μg; pCXLE-hUL, pCXLE-hSK, pCXLE-hOCT3/4-shp53-F, and pCXWB-EBNA1) by AMAXA 4D Nucleofector (LONZA) as previously described [21]. 6 days postnucleofection, 2×105 cells were replated on a matrigel-coated 35 mm dish with DMEM containing 10% FBS. After 24 h of replating, the medium was switched to the human reprograming medium (ReproEasy, Cellapy, CA5001500) and changed every other day. 2 weeks after transduction, the medium was changed daily with hESC medium until iPSC colonies were observed. The generated iPSCs colonies were picked manually and maintained in feed-free matrigel-coated dishes. The iPSCs were fed every other day and were passaged 1:5–10 every 5 days using Versene

(Invitrogen). All the protocol was approved by the Medical Research Ethics Committee of Wenzhou Medical University (2017–066) and written informed consent was obtained from the patients.

2.3. Characterization of iPSCs (Undifferentiation and Multidifferentiation). Alkaline Phosphatase (AP) Staining Kit II (Beyotime, C3206) was used for AP staining of iPSCs as per the manufacturer's instructions. Briefly, iPSCs were fixed with 4% paraformaldehyde at room temperature for 5 min after PBST wash. Then cells were incubated in AP substrate solution for 15 min, to stop the reaction by washing with PBS. For immunofluorescence staining, iPSCs or differentiated cells were fixed in 4% paraformaldehyde for 20 min, permeabilized and blocked using 0.5% Triton X-100 in PBS with 5% normal goat serum, and incubated overnight with the primary antibodies: rabbit anti-OCT4, rabbit anti-SOX2, rabbit anti-Nanog, mouse anti-TRA-1-60, mouse anti-TRA-1-81 (1:100, Stemgent), mouse anti-TUJ1 (1:500, Covance), rabbit anti-α-1-fetoprotein (1:400, Abcam), mouse anti-smooth muscle α-actin (α-SMA) (Sigma), mouse anti-calponin (CNN, Sigma), rabbit anti-smooth muscle 22 α (SM22α) (Abcam). Secondary goat-anti-mouse and anti-rabbit IgG antibodies conjugated with Alexa 488 or Alexa 594 were added to the samples and incubated for 1 h. The cell nuclei were stained with 4′,6-diamidino-2-phenylindole (DAPI, Life Technologies). Cells were rinsed, and fluorescence was analyzed using a Nikon (Ts2-FL) microscope.

2.4. Teratoma Formation Assay. Immunodeficient SCID mice were injected 1 x 106 iPSCs with DMEM/Matrigel solution into the hind limbs intramuscularly. 8 weeks after injection, the teratomas were dissected and fixed with 4% paraformaldehyde. Paraffin-embedded tissue was sliced and stained with hematoxylin and eosin. After the experiment, euthanasia was performed on SCID mice using the carbon dioxide (CO_2) inhalation method. The CO_2 flow rate was set at 5 L/min, with a total exposure time of 4 min. The success criteria for euthanasia were the cessation of respiration, disappearance of hindlimb reflexes, and loss of corneal reflexes. The animal procedures were performed according to the protocol approved by the Laboratory Animal Ethics Committee of the Ethics Committee of Wenzhou Medical University (XM592002-017).

2.5. SMC Differentiation From iPSCs. SMC differentiation from iPSCs was performed according to our previous human ES cells protocol with minor modification [22]. iPSCs were digested with 1 mg/mL collagenase IV (Solarbio) for 15–20 min and transferred to the ultra-low-attachment dish (corning) to make embryoid bodies (EBs). EBs were cultured in a human ES cell medium without bFGF. 6-day-old EBs were replated to 35 mm dishes coated with 0.1% gelatin and cultured for 6–12 days in DMEM with 10% FBS. The outgrowth cells from EBs were dissociated with TrypLE express and cultured on Matrigel-coated 35 mm dishes with smooth muscle growth medium2 (SmGM2, Lonza). Cells were passaged when they reached 80%–90% confluence. To induce differentiation to SMCs, cells were cultured on differentiation conditions, in which cells were grown in gelatin-coated dishes in SmGM2 basal medium with 5% FBS for 5 days.

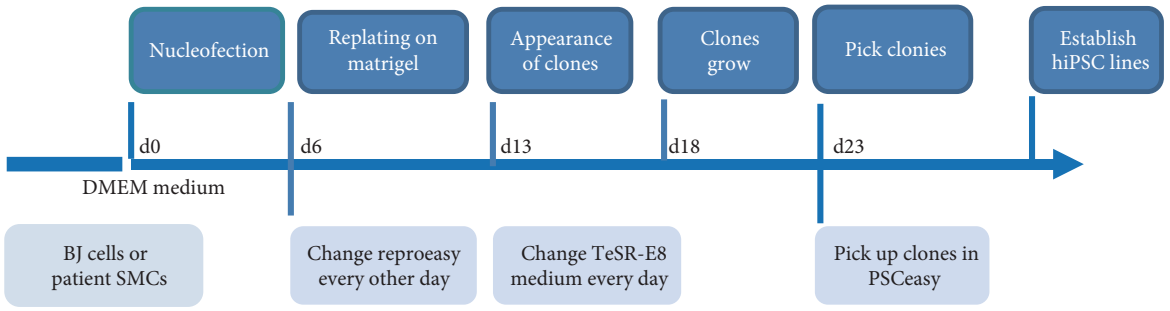
2.6. Contractility Assay. After 5 days of differentiation, SMCs were washed with phosphate-buffered saline (PBS), stimulated with 1 mM carbachol in smooth muscle differentiation medium, and monitored for 30 min as we described before [22]. Images of the same field were collected every 1 min for 30 min and compiled into movies using the Olympus software (DP controller). To analyze the change in cell surface area between 0 min and 30 min using ImageJ software.

2.7. Quantitative RT–PCR. Total RNA was extracted using the RNeasy Mini kit (Qiagen). cDNA was synthesized from 1 μg of RNA with a PrimeScript RT reagent kit (Takara, RR037A). Pluripotency genes were amplified with gene-specific primers by PCR using Taq DNA polymerase (NEB, M0267V) in a SimpliAmp Thermal Cycler (Applied Biosystems). Real-time PCR was performed on a StepOne Plus Real-Time System (Life Technologies) using iTaq Universal SYBR Green Supermix (Bio-Rad) as previously described [23]. Quantification of gene expression was assessed with the comparative cycle threshold (Ct) method. The relative amounts of mRNA for the different genes were determined by subtracting the Ct values for these genes from the Ct value for the housekeeping gene GAPDH (ΔCt).

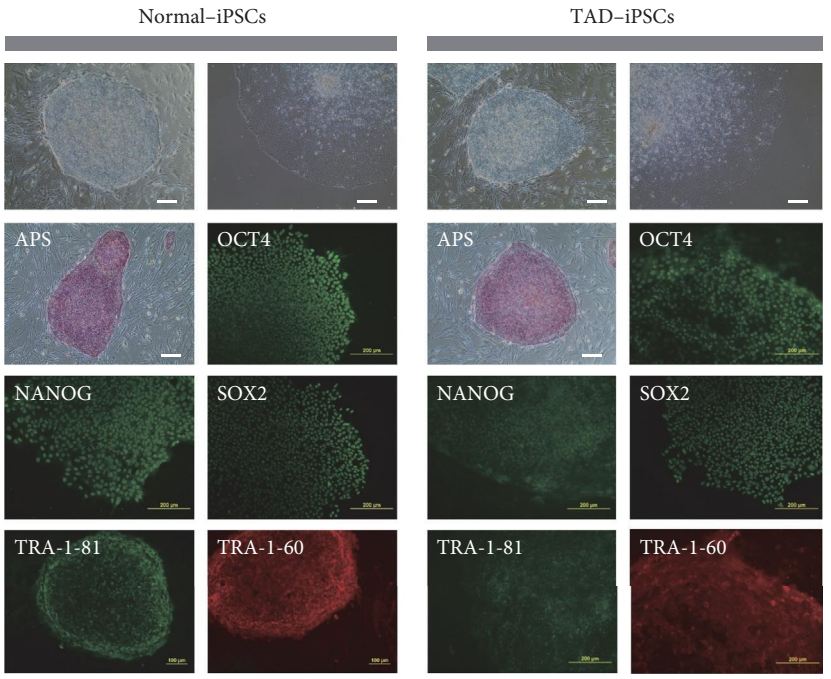
2.8. Flow Cytometry. Cells were dissociated with 0.05% trypsin into single cells and suspended in PBS, then fixed with the fixation solution from the Fixation/Permeabilization kit (BD Biosciences), and stained with primary and detection antibodies as described by the manufacturer. Briefly, the dissociated cells were resuspended (5×105 cells) in 250 μL of fixation/permeabilization solution, kept at room temperature for 30 min, and washed twice with Perm/Wash buffer. After blocking with blocking solution for 30 min, the cells were incubated with the primary antibody for 1 h on ice. The cells were then resuspended in 100 μL of Perm/Wash buffer after incubation with a secondary antibody for 1 h on ice, washed twice, and analyzed by flow cytometry.

2.9. Karyotyping. Karyotyping of iPSC was performed on G-band metaphase chromosomes by Nuwacell Ltd. The proliferating iPSCs were blocked by 50 ng/mL of colcemid for 2 h, digested with trypsin-EDTA, and then treated with hypotonic KCl solution for 20–40 min at 37°C. Glass slides were prepared with three steps of fixation in methanol/glacial acetic acid (3:1). QFQ-banding was analyzed at a resolution of 400 bands per haploid genome according to the International System for Human Cytogenetic Nomenclature (ISCN2016).

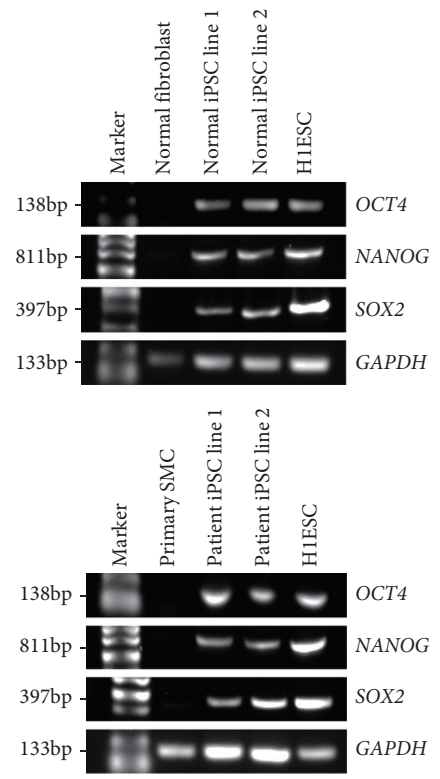
2.10. Western Blotting Analysis. Cells were lysed in RIPA buffer on ice, and protein concentrations were determined by BCA protein assay (Thermo Scientific, Rockford, IL) according to the manufacturer's protocol. 30 μg of cell lysate was resolved by 10% sodium dodecyl sulfate (SDS)-polyacrylamide gel and transferred to nitrocellulose (NC) Protran membranes (Whatman, Dassel, Germany). Blots were incubated for 1 h at RT in blocking buffer (5% milk in tris-buffered saline [150 mM NaCl, 10 mM Tris, pH8.0, 0.1%



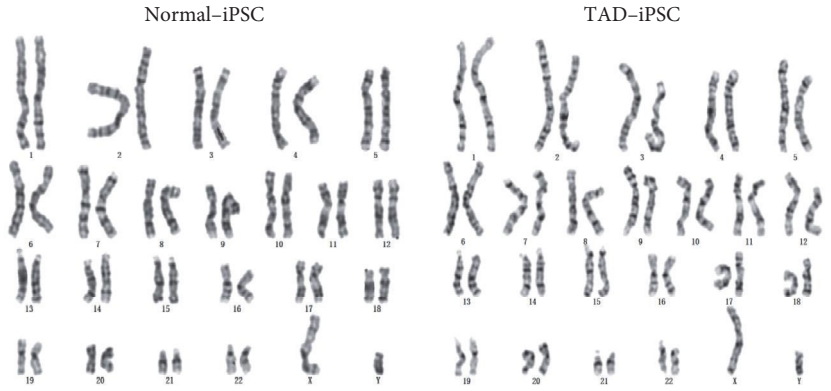
(A)



(B)

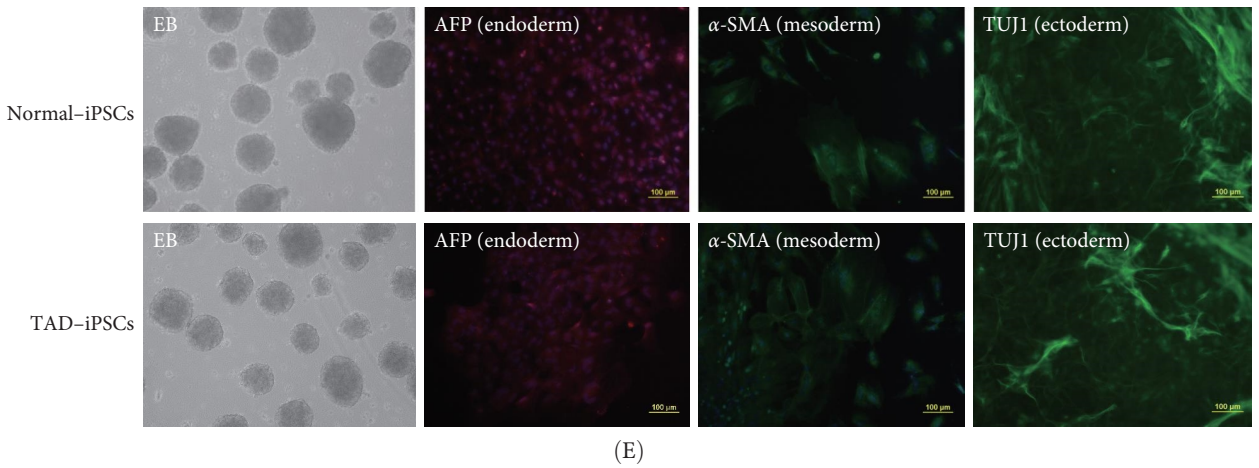


(C)

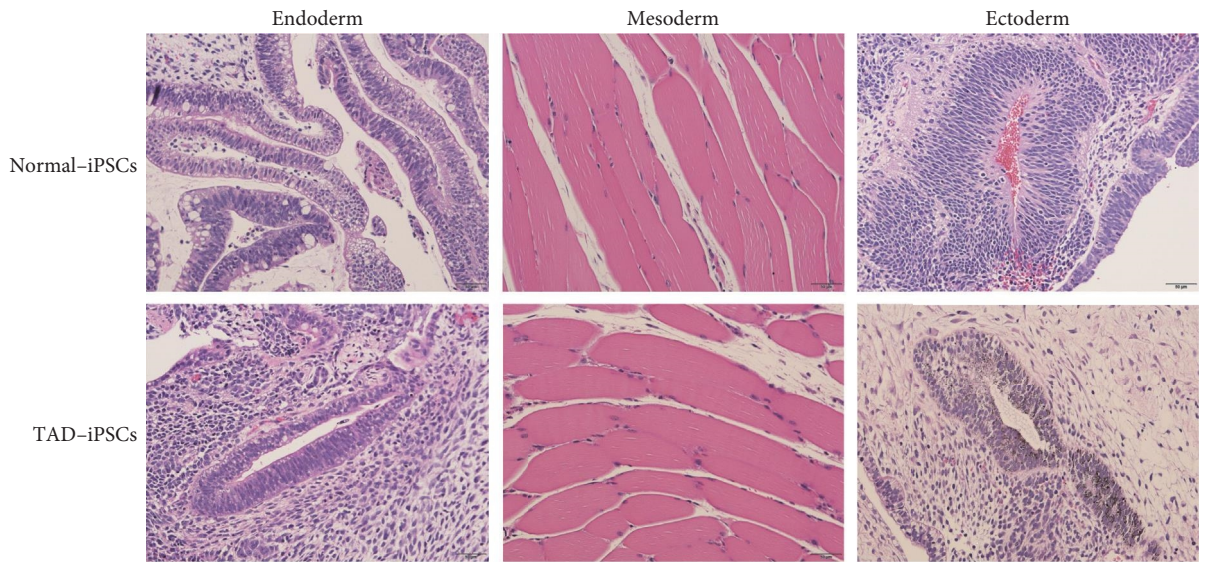


(D)

Figure 1: Continued.



(E)



(F)

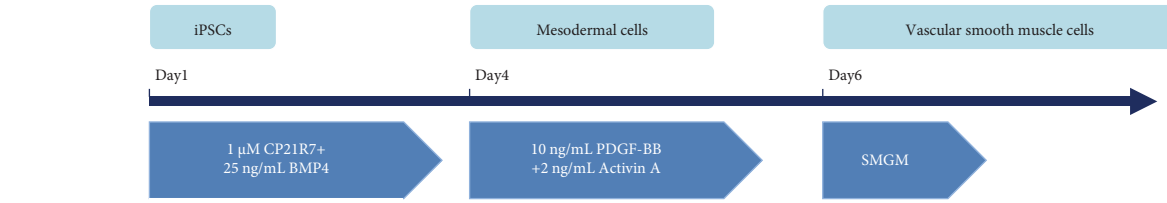
Figure 1: Generation and characterization of hiPSCs from TAD patients and normal cells. (A) Schematic diagram of nonintegrative iPSCs reprograming mediated by episomal vectors. (B) The morphology of established iPSC clone, alkaline phosphatase staining (APS), and immunofluorescence staining with pluripotency markers, including, OCT4, NANOG, SOX2, TRA-1-60, and TRA-1-81. Scale bar = 200 μm. (C) Pluripotency marker gene expression assessed by RT–PCR. (D) Karyotyping analysis of both normal iPSCs and TAD–iPSCs. (E) In vitro EB-mediated differentiation of iPSCs into three germ layers, shown by immunofluorescence staining of AFP (endoderm), α-SMA (mesoderm), TUJ1 (ectoderm). Scale bar = 200 μm. (F) Hematoxylin and eosin (HE) staining of teratoma derived from both normal and TAD iPSCs, scale bar = 50 μm.

Tween-20]), and with primary antibody overnight at 4°C, followed by horseradish peroxidase-conjugated secondary antibody (1:20,000 in blocking buffer) for 1 h at RT, and visualized by SuperSignal West Pico Chemiluminescent substrate (Thermo Scientific, Rockford, IL) and were detected using a digital gel image analysis system (Bio-Rad, Hercules, CA, USA). The density of the protein bands was normalized to the GAPDH and presented as a percentage increase.

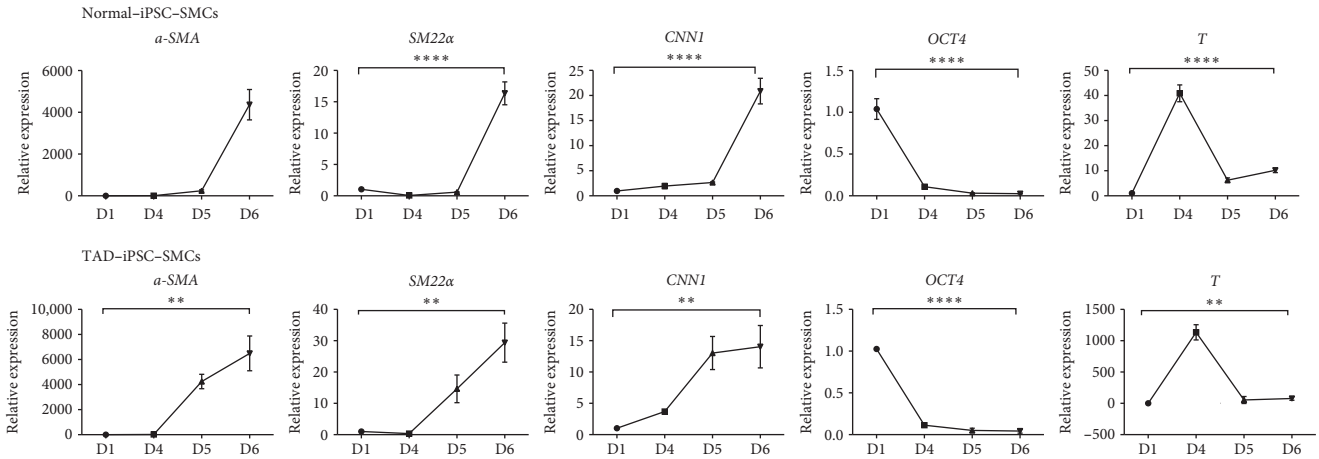
2.11. Statistics. Statistical analyses were performed using Prism (GraphPad Software, Inc., La Jolla, CA). Numerical data were reported as mean ± s.e.m. From triplicate cell culture ($n = 3$), the Student's t-test was applied to test the significance between the groups. The value of $p < 0.05$ was considered statistically significant.

3. Results

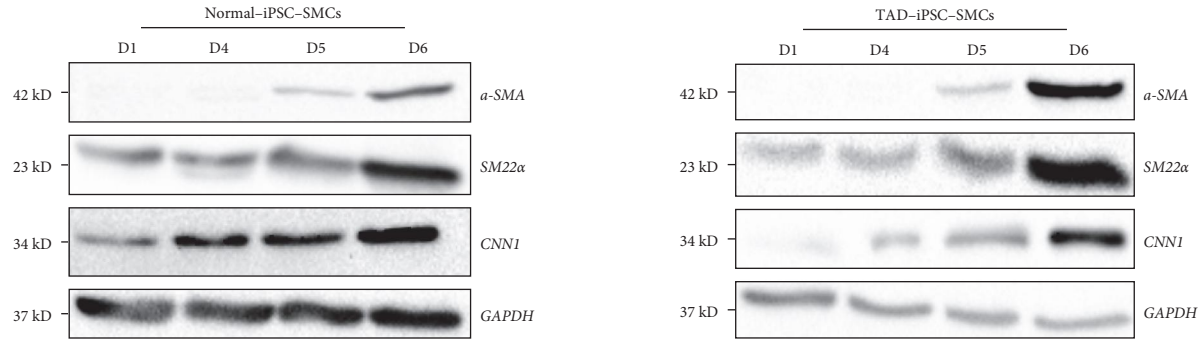
3.1. Generation and Characterization of Nonintegrated iPSCs From TAD Patient. The generation of integration-free iPS cells is crucial for disease modeling, cell-based therapy, and regenerative medicine. Using our previously established episomal vector-mediated human iPSCs reprograming platform, we generated nonintegrative iPSCs from a 47-year-old patient with TAD (Figure 1 and Supporting Information: Figure S1). Additionally, we also generated a normal iPSC

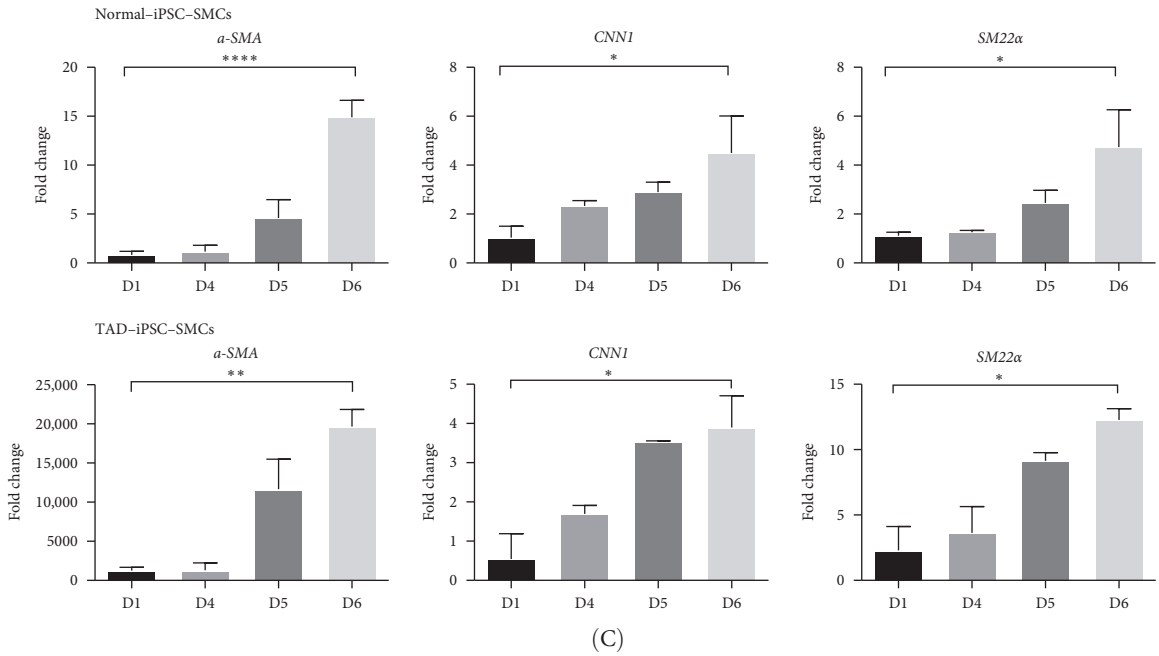


(A)



(B)





(C)

Figure 2: Continued.

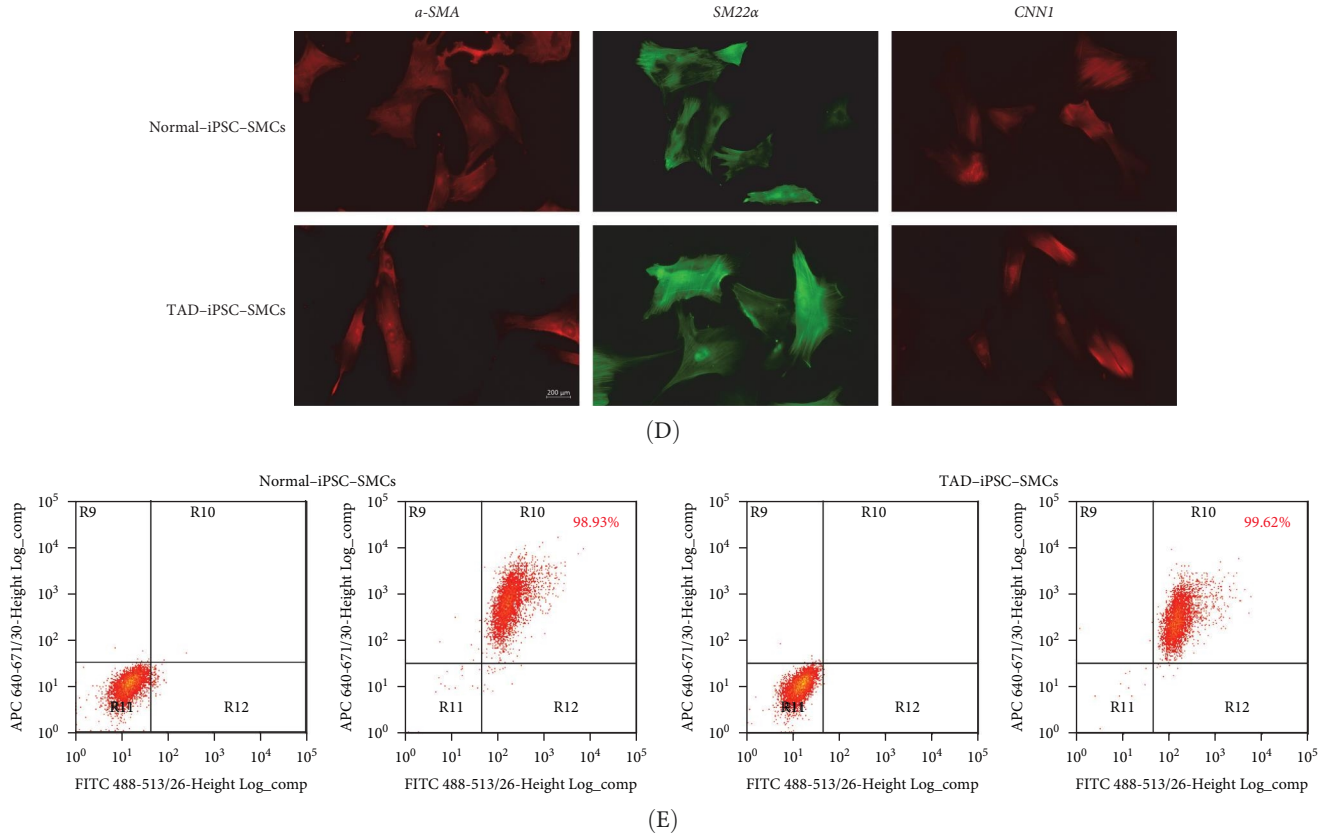
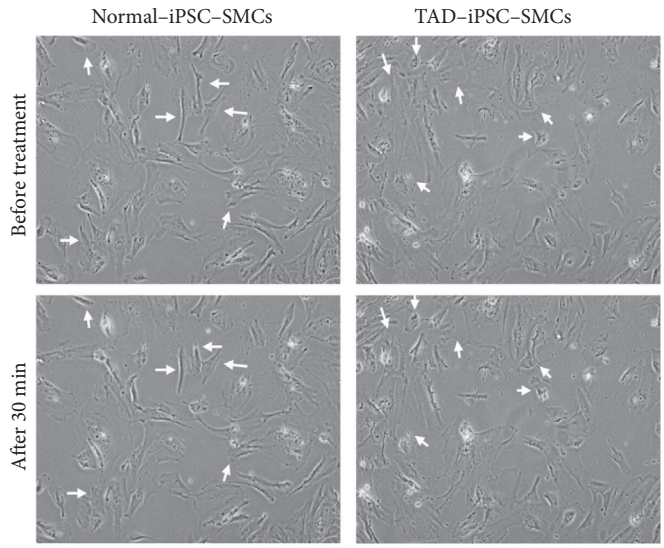


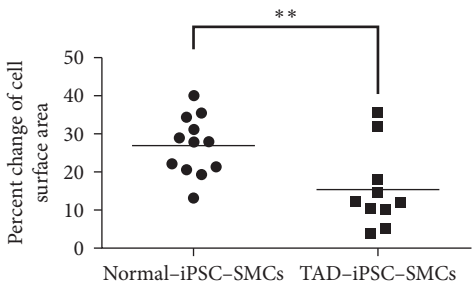
Figure 2: Mesoderm-mediated SMC differentiation. (A) Schematic illustration of the SMC differentiation from iPSCs. (B) SMC marker gene expression during SMC differentiation from normal and TAD–iPSCs. (C) Protein expression of SMC marker genes during SMC differentiation from normal and TAD–iPSCs by West blotting. (D) immunofluorescence staining of SMC marker genes in normal and TAD–iPSCs. (E) Flow cytometry results for iPSC–SMC differentiation. Data are shown as the mean ± S.D. for at least three independent experiments. $^{*}p<0.05$, $^{**}p<0.01$, $^{****}p<0.0001$.

from BJ cells, which are normal human dermal fibroblasts (Figure 1 and Supporting Information: Figure S1). We picked different colonies to establish at least three lines for each sample based on their ESC-like morphology. We characterized the pluripotency of these iPSC lines using AP staining (APS) and immunofluorescence. Figure 1B shows a representative TAD–iPSC and normal iPSC lines with positive APS staining and expression of pluripotency markers, including the transcription factor OCT4, NANOG, and SOX2, as well as the cell surface proteins TRA-1-60 and TRA-1-81. RT–PCR analysis confirmed that the pluripotency genes of OCT4, NANOG, and SOX2 were highly expressed in all the iPSC lines (Figure 1C). Karyotyping assays confirmed that both the normal iPSCs and TAD- iPSCs exhibited a normal karyotype (Figure 1D). To further characterize the pluripotency of normal and TAD–iPSCs, we assessed their differentiation potential into the three germ layers in vitro. We used antibodies for α-fetoprotein (AFP), smooth muscle α-actin (α-SMA), and TUJ1 to determine endoderm, mesoderm, and ectoderm differentiation, respectively. As shown in Figure 1E, both normal and TAD–iPSC lines could differentiate into three layers in vitro. When these iPSCs were inoculated into SCID mice, they formed teratomas in vivo. Histological staining of these teratomas indicated the presence of various tissues representing all germ layers, including neural rosette (ectoderm), muscle (mesoderm), and gut-like epithelial (endoderm, Figure 1F).

3.2. SMC Differentiation From TAD–iPSCs. VSMCs play a central role in the pathogenesis of TAD [12]. To investigate the functions of VSMC in TAD, we differentiated both TAD- and normal-iPSCs into VSMCs following our recent protocol [23]. Initially, iPSC lines were differentiated into mesodermal cells over 3 days and subsequently induced into VSMCs using PDGF-BB and activin A in another 3 days (Figure 2A). Throughout this process, we did not observe a significant difference in the differentiation potential between the two groups. Both normal- and TAD–iPSC lines showed increased expression of the SMC marker genes, including α-SMA, SM22α, and CNN, along with decreased expression of the pluripotency marker OCT4, as determined by RT–qPCR (Figure 2B). We further verified the increased expression of VSMC genes α-SMA, SM22α, and CNN through immunoblotting (Figure 2C). The differentiated VSMCs were maintained in SMGM, and the expression of VSMC differentiation markers was further confirmed by immunofluorescence staining



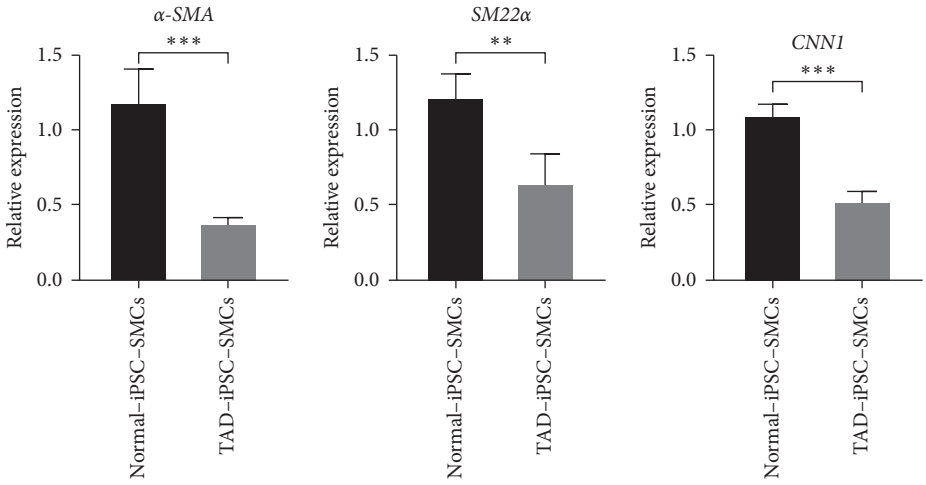
(A)



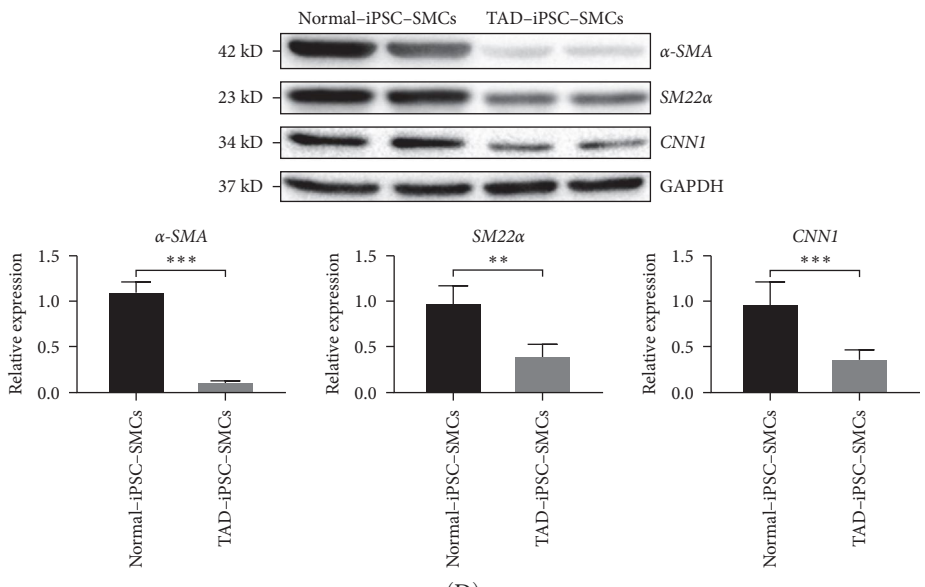
	Percent change of cell surface area
Normal–iPSC–SMCs	26.96 ± 2.25 ($N = 12$)
TAD–iPSC–SMCs	15.42 ± 3.32 ($N = 10$)

($P = 0.0078$)

(B)



(C)



(D)

Figure 3: Continued.

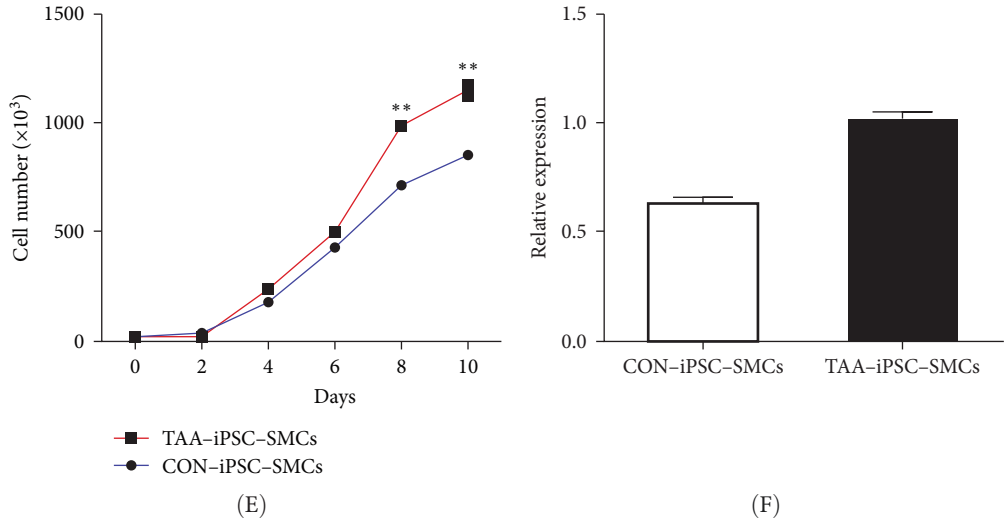


FIGURE 3: TAD–iPSC–SMCs reduce contractile ability and increase proliferation compared to control-iPSCs–SMCs. (A) TAD–iPSC–SMCs reduce contractile ability compared to normal-iPSCs–SMCs. TAD–iPSC–SMCs were treated with carbachol (1 mM) and images were recorded every 1 min for consecutive 30 min. (B) Quantitate iPSCs-derived SMC contraction assay. (C) Comparison of SMC marker gene expression levels in normal and TAD–iPSC–SMCs. (D) Immunoblot analysis and quantification of SMC marker gene expression in normal and TAD–iPSC–SMCs. (E) TAD–iPSC–SMCs show a higher proliferation rate compared to normal-iPSC–SMCs, as indicated by the growth curve. (F) MTT assay confirmed the higher proliferation ability in TAD–iPSC-SMCs. Data are shown as the mean ± S.D. for at least three independent experiments. $^{*}p<0.05$, $^{**}p<0.01$, $^{***}p<0.001$.

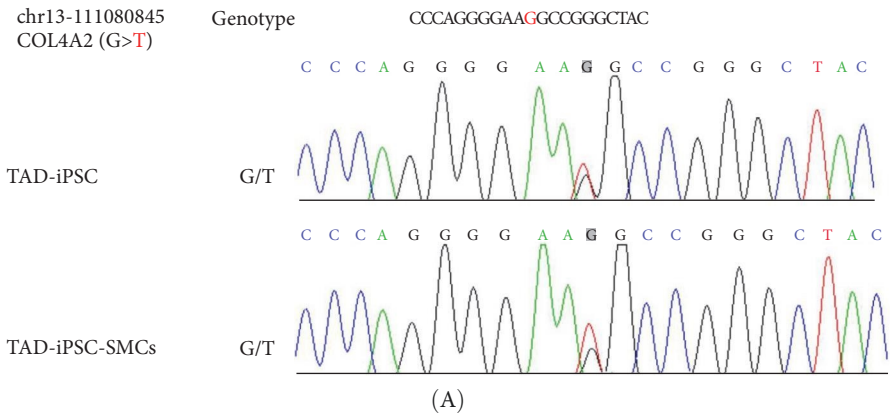
(Figure 2D). Additionally, flow cytometry analysis showed that the majority of differentiated cells expressed α-SMA (Figure 2E).

3.3. TAD–iPSC–SMCs Reduced the Contractile Ability and Increased Proliferation Rate. Previous studies have reported that SMC from TAD patients exhibit dysfunction [24]. To investigate whether TAD–iPSC-derived SMCs (TAD–iPSC-SMCs) exhibit similar issues, we first examine their contraction ability. of TAD–iPSC-SMCs is dysfunctional. The cells were treated with carbachol, an agonist against acetylcholine receptors, for 30 min. This treatment induced contraction, which resulted in a change in cell surface area on the dishes. TAD–iPSC–SMCs showed a lower contractile rate in response to carbachol compared to normal-iPSC–SMCs (Figure 3A,B). Consistently, both the protein and mRNA expression levels of SMC contractile proteins, including α-SMA, SM22α, and CNN, were decreased in TAD–iPSC–SMCs compared to normal-iPSC–SMCs (Figure 3C,D). Additionally, TAD–iPSC–SMCs exhibited a greater proliferation capacity than normal-iPSC–SMCs, as demonstrated by the proliferation curve and confirmed by the MTT assay (Figure 3E,F). These results suggest that SMCs in TAD–iPSC–SMCs may undergo phenotypic switching, consistent with previous reports [25].

3.4. TAD–iPSC–SMCs Show Abnormal Collagen Expression. To identify the potential genetic defect underlying the abnormal function of TAD–iPSC–SMCs, we performed whole exome sequencing of PBMCs from the TAD patient. Intriguingly, we found a mutation in the COL4A2 gene among several predicted impaired mutations that we suspected might be associated with TAD. Sanger sequencing confirmed the COL4A2 R131M (c.392 G > T) mutation in both TAD–iPSCs and the derived SMCs (Figure 4A). The R131 residue of COL4A2 is relatively conserved across several mammalian species (Figure 4B). COL4A2 encodes the collagen type IV α2 chain, and its mutations have been linked to various cardiovascular diseases, including aneurysms [26, 27]. Using a web-based prediction tool, we found that the COL4A2 R131M mutation is predicted to be harmful (Figure 4B). We then examined the expression of several vascular collagen genes in both normal- and TAD–iPSC–SMCs. Our results showed that the expression of COL4A2 and COL4A1 was decreased in TAD–iPSC–SMCs compared to normal iPSC–SMCs, while the expression of COL1A1 and COL3A1 genes was increased (Figure 4C,D). When SMCs were exposed to TGF-β, all collagen genes except for COL4A2 showed increased expression (Figure 4C). These findings suggest that the COL4A2 mutation might contribute to the phenotype observed in TAD–iPSC–SMCs.

3.5. Noncanonical TGF-β Signaling Activated in TAD–iPSC–SMCs. To determine whether TGF-β signaling contributes to the progression of the TAD phenotype, we examined both the canonical TGF-β-Smad and noncanonical TGF-β-ERK signaling pathways in TAD–iPSC–SMCs. We observed that the level of phosphorylated ERK1/2 (pERK1/2), but not phosphorylated SMAD2 (pSMAD2), was higher at the basal level in TAD–iPSC–SMCs compared to normal iPSC–SMCs (Figure 5A). Additionally, TAD–iPSC–SMCs exhibited less pSMAD2 activation following TGF-β stimulation.

We also compared the expression levels of MMPs in normal- and TAD–iPSC–SMCs. Among the MMPs



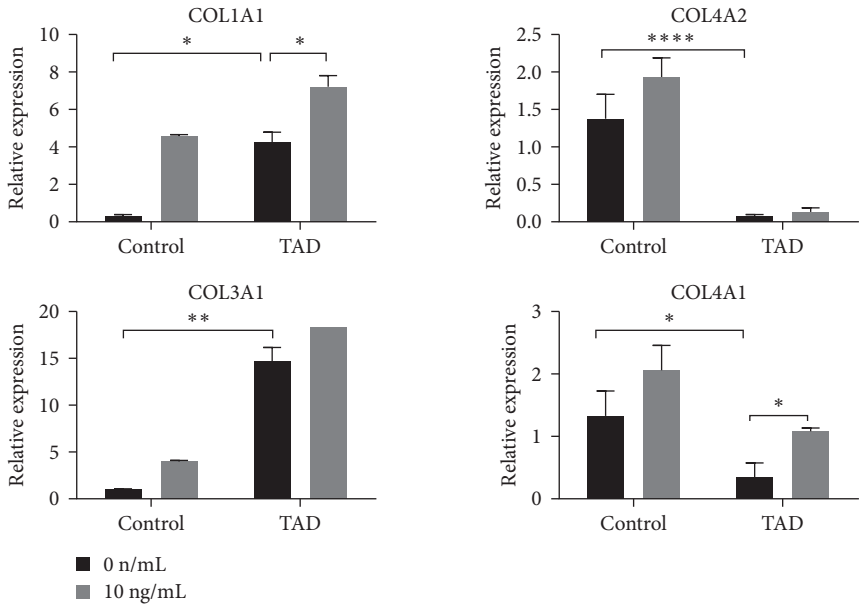
(A)



PGHPGQGGPRGRPGYDGCNGT *Homo sapiens*
PGHPGQGGPRGRPGYDGCNGT *Rattus norvegicus*
PGHPGQGGPRGRPGYDGCNGT *Mus musculus*
PGHPGQGGPRGRPGYDGCNGT *Pan troglodytes* (Chimpanzee)
PGHPGQGGPRGRPGSDGCNGT *Sus scrofa* (pig)
PGHPGT AGPRGRPGVDGCNGT *Gadus morhua* (cod)

Gene	Chromo-some	AAChange.refGene	Genotype	Variant allele frequency	Pathogenesis prediction	Pathogenicity analysis	Geredity	Phenotype
COL4A2	Chr13-111080845	NM_001846; exon7;c.392 G>T(p.R131M)	Het	0.00002	Harmful	Uncertain	AD	Porencephaly

(B)



(C)

Figure 4: Continued.

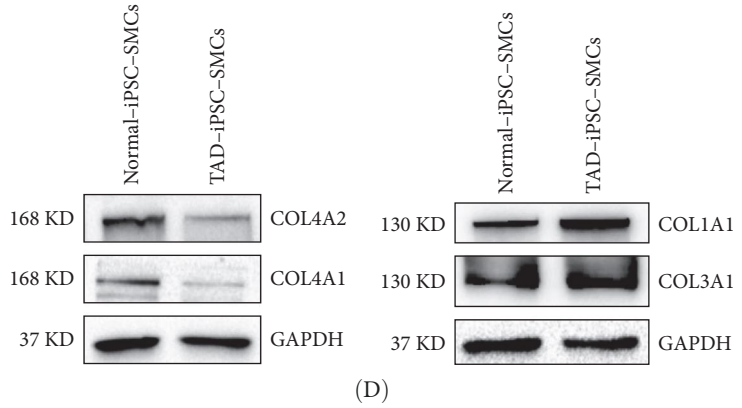


FIGURE 4: TAD–iPSC and derived SMCs carry a mutation in collagen type IV (*COL4A2*). (A) Sanger sequencing of collagen IV A2 (COL4A2) mutation (c.392G > T, p. R131M) in the TAD–iPSC line and the derived SMCs. (B) Schematic structure of COL4A2 showing the mutation R131M located in the 7S domain, which is relatively conserved among several mammal species. (C) Expression of various types of collagen in both normal and TAD–iPSC–SMCs, with and without TGF-β treatment. (D) Protein expression level of COL4A2 and COL4A1 decreases, while COL1A1 and COL3A1 increased. Data are shown as the mean $\pm$ S.D. for at least three independent experiments. $^{*}p<0.05$, $^{**}p<0.01$, $^{****}p<0.0001$.

examined, only MMP9 showed relatively higher expression in TAD–iPSC–SMCs. However, treatment with the cytokine IL-1β for 24 h elevated the mRNA expression levels of MMP2, MMP3, MMP9, and MMP12 in both normal and TAD–iPSC–SMCs (Figure 5B). These results suggest that TAD–iPSC–SMCs exhibit an imbalance between the canonical Smad2-dependent and noncanonical ERK1/2-dependent TGF-β signaling pathways.

4. Discussion

In this study, we established iPSCs from a TAD patient and differentiated them into SMCs to create a disease cellular model for investigating the molecular mechanisms of human TAD. Using this patient-specific iPSC and SMC differentiation platform, we discovered that TAD–iPSC–SMCs exhibited reduced contraction ability and increased proliferation rate, indicative of phenotypic switching as early events in aortic dissection. Additionally, we identified a COL4A2 mutation in this patient, with TAD–iPSC-derived SMCs showing reduced COL4A2 expression but increased expression of COL1A1 and COL3A1. Furthermore, our model revealed dysfunctional TGF-β signaling, characterized by inhibited canonical Smad2-mediated pathways and activated noncanonical ERK1/2-mediated pathways in SMCs.

The derivation of human iPSCs has provided unprecedented opportunities for cardiovascular disease modeling and regenerative medicine [28]. Previous studies have demonstrated the application of iPSCs in modeling various cardiovascular diseases, such as long-QT syndrome and arrhythmogenic right ventricular dysplasia [29, 30]. Recently, the Sinha group developed an in vitro MFS-iPSC model, using iPSC-derived smooth muscle cells to elucidate the role of TGF-β signaling in MFS pathogenesis, and identified a novel role of p38 and KLF4 in the MFS pathogenesis [18]. Our study extends this approach to TAD, demonstrating that TAD–iPSC-SMCs faithfully mimic human SMC phenotypes associated with TAD. This model adds to the growing list of iPSC-based disease models and offers a potential platform for screening novel therapeutics for TAD.

The ECM, particularly collagen, is crucial in the pathogenesis of TAD. Collagen I and III, the most abundant fibrous collagens in the aortic wall, are essential for tensile strength and cytokine sequestration. Dysfunction of collagen III is linked to TAD in Ehlers–Danlos syndrome (vascular type IV, OMIM#130050). Although some studies have reported increased collagen I and III expression in TAD, de Figueiredo Borges et al. observed decreased collagen in the outer half of the dissected aortic wall [31], suggesting that collagen content in the media may decrease prior to dissection. Interestingly, type IV collagen, a basement membrane-specific type, is also implicated in TAD. Microarray data from the Sandmann group identified downregulation of COL4A2 and COL4A5 in aortic dissection [11].

Consistent with these findings, we observed decreased COL4A2 expression in TAD–iPSC-SMCs and identified a COL4A2 R131M mutation in the patient. This mutation may weaken the tunica intima by reducing collagen IV expression, contributing to TAD formation. Variants of collagen genes, including COL4A2, have been implicated in sporadic AD pathogenesis [32], and COL4A1 and COL4A2 mutations are associated with a broader spectrum of cardiovascular, renal, ophthalmological, and muscular abnormalities as well as aneurysms [27, 33]. A recent study reported that a loss-of-function mutation in lysyl oxidase (LOX), an enzyme critical for collagen cross-linking, causes TAA and dissection [34], supporting our hypothesis that mutations in collagen-encoding genes may weaken the aortic wall and lead to dissection formation.

In healthy vascular walls, SMCs maintain vascular tone and remain quiescent in the contractile phenotype. Under pathological conditions, SMCs can dedifferentiate into a synthetic phenotype and proliferate. This phenotypic switching is recognized as an early event in TAA formation [14], characterized by downregulation of VSMC differentiation markers such as SM22α and smooth muscle α-actin. Our findings in TAD patient-specific iPSC–SMCs are consistent with this observation (Figure 3C,D). This is consistent with our current result in the TAD patient-specific iPSC–SMC.

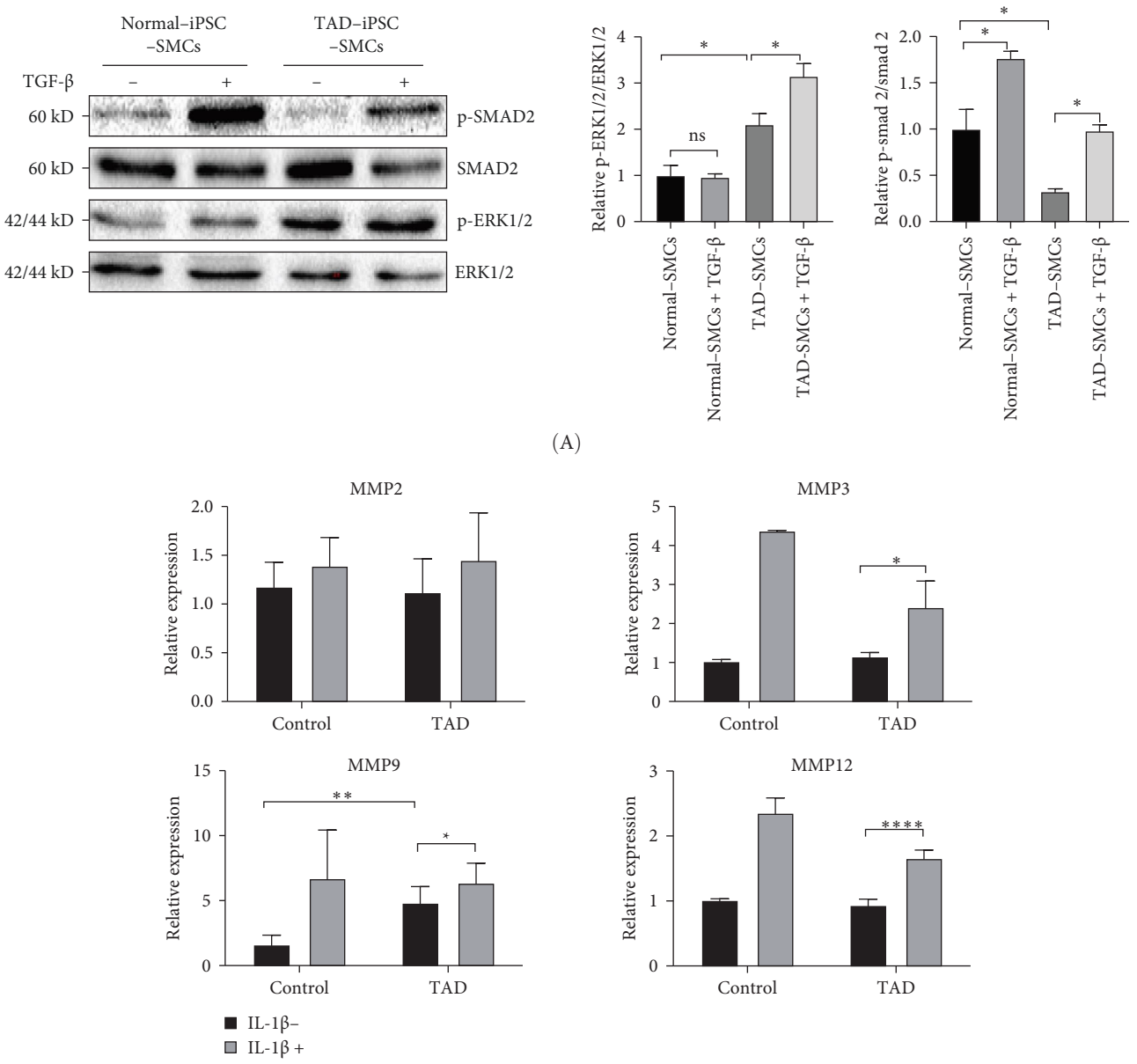


Figure 5: Noncanonical TGF-β signaling is activated and MMP9 expression is increased in TAD–iPSC–SMCs. (A) Western blotting analysis of phosphorylated TGF-β canonical (SMAD2) and noncanonical (ERK1/2) pathways in normal and TAD–iPSC–SMCs with or without TGF-β treatment. (B) RT–qPCR expression of MMPs in normal and TAD–iPSC–SMCs with or without IL-1β (10 ng/mL) treatment. Data are shown as the mean ± S.D. for at least three independent experiments. $^{*}p<0.05$, $^{**}p<0.01$, $^{****}p<0.0001$.

The Milewicz group reported that TGFBR2 mutations lead to decreased expression of SMC contractile proteins, suggesting that defective SMC contractile function contributes to TAAD pathogenesis [35]. Although the underlying mechanisms remain unclear, recent research indicates the pivotal role of the XBP1u-FoxO4-myocardin axis in maintaining the VSMC contractile phenotype and preventing phenotypic switching during aortic aneurysm formation [36]. ER stress pathways, potentially involved in aortic dissection or aneurysm, may also be implicated, as suggested by previous studies [37]. Although COL4A2 mutations may also cause ER stress, we did not investigate this pathway in our study.

TGF-β signaling plays a crucial role in TAD development. This multifunctional signaling molecule is involved in various physiological processes, including SMC differentiation, ECM synthesis, and degradation via upregulation of MMPs. TGF-β activates both Smad2/3-mediated canonical pathways and non-Smad-mediated (noncanonical) pathways. Initial studies suggested that excessive TGF-β signaling contributes to TAD and aneurysm [38]. Habashi et al. [39] reported that the onset of thoracic aortic disease in Fbn1C1039/+ mice is associated with increased TGF-β signaling, which can be prevented by TGF-β inhibition or AT1R blockade with losartan. Patients with mutations in genes such as α-SMA, MYH11, and

fibulin-4 also exhibit TGF-β hyperactivity [40]. Furthermore, patients and mice with heterozygous loss-of-function mutations in genes encoding components of canonical TGF-β signaling pathway, such as ligands, receptors, and signal transducers, also found overactivation of TGF-β signaling. Conversely, recent evidence suggests that TGF-β signaling may protect against aortic aneurysm and dissection. Li et al. and Wei et al. [41, 42] found that Tgfbr2 disruption in smooth muscle cells exacerbates aneurysm and dissection in MFS mice, indicating that TGF-β signaling is essential for postnatal aortic growth and homeostasis. TGF-β could activate intracellular smad-dependent canonical pathway and smad-independent noncanonical pathways (e.g., ERK1/2, JNK). While inhibition of noncanonical TGF-β signaling ameliorates aortic aneurysm progression in MFS mice [43], our iPSC–SMC model showed hyperactivation of noncanonical ERK1/2 signaling and reduced Smad2 activity in response to TGF-β in patient-derived SMCs (Figure 5A). This imbalance between noncanonical and canonical TGF-β signaling likely contributes to aortic dissection or aneurysm development.

However, our study has some limitations. For example, in this study, we only included one patient sample carrying the target COL4A2 mutation. The genetic background of human individuals is extremely complex, and even for the same disease, there may be significant genetic heterogeneity among different patients. This makes it impossible for us to fully determine whether the observed abnormal VSMC phenotype is directly caused by the COL4A2 mutation alone or is to some extent modulated by other genetic variations in the unique genetic background of the patient. For example, the patient may simultaneously carry other gene polymorphisms or mutations related to VSMC function, and these genetic factors may interact with the COL4A2 mutation to affect the VSMC phenotype. The lack of an isogenic iPSCs model carrying the corrected COL4A2 mutation is another important limitation. In this study, due to the complexity of the technical operation, such as the great challenge in obtaining efficient homologous recombination efficiency, it is necessary to optimize CRISPR-Cas9 and other gene editing systems to improve editing efficiency; at the same time, the screening and identification of corrected cell clones also require a lot of time and energy to ensure that the obtained clones are successfully corrected and have no other off-target effects, which has prolonged the experimental cycle. Therefore, at the stage of this study, we have not completed the construction of this model. This makes it impossible for us to directly prove whether the dysfunction of VSMC can be restored when the COL4A2 mutation is corrected, thus to a certain extent weakening the persuasiveness of the causal relationship between the COL4A2 mutation and VSMC dysfunction.

In summary, our work has modeled the TAD-associated SMC mechanism using patient-specific iPSCs. Our study suggests that TAD–iPSC–SMCs carrying a COL4A2 mutation may exhibit phenotypic switching and activation of noncanonical ERK1/2 TGF-β signaling, which could potentially contribute to TAD progression. Our findings highlight the potential importance of the noncanonical TGF-β pathway in TAD pathogenesis and suggest that targeting this pathway could be a therapeutic strategy for TAD treatment in the future.

Data Availability Statement

The original contributions presented in the study are included in the article/Supporting Information, further inquiries can be directed to the corresponding authors.

Ethics Statement

This study was approved by the medical research ethics committee of Wenzhou Medical University (Approval number: 2017-066). The study was conducted in accordance with the local legislation and institutional requirements.

Consent

The authors have nothing to report.

Disclosure

A preprint has previously been published [44].

Conflicts of Interest

The authors declare no conflicts of interest.

Author Contributions

Peifeng Jin: formal analysis, investigation, methodology, visualization, writing – original draft, writing – review and editing. **Yubin Xu**: formal analysis, data curation, investigation, writing – original draft, writing – review and editing. **Sixian Wang**: formal analysis, data curation, investigation, writing – review and editing. **Lu Ding**: data curation, formal analysis, writing – review and editing. **Yuhao Chen**: investigation, writing – review and editing. **Miqi Zhou**: investigation, writing – review and editing. **Xiufang Chen**: funding acquisition, investigation, methodology, writing – review and editing. **Xiaofang Fan**: project administration, resources, writing – review and editing. **Yongsheng Gong**: supervision, validation, writing – review and editing. **Ming Li**: supervision, validation, writing – review and editing. **Yongyu Wang**: conceptualization, visualization, funding acquisition, investigation, supervision, writing – original draft, writing – sreview and editing. Peifeng Jin and Yubin Xu contributed equally to this work and share first authorship.

Funding

The authors declare financial support was received for the research, authorship, and/or publication of this article. This work was supported by the National Natural Science Foundation of China (Grants 82070487, 32370787, 81670454), the Scientific Research Start-up Fund of Wenzhou Medical University (Grant QTJ15029), and the Wenzhou Major Science and Technology Innovation Project (Grant ZY2021014).

Acknowledgments

We would like to thank all the members of the Institute of Hypoxia Medicine, the patient, and his family who contributed to this work. We appreciate the great help from Dr. Jiaxi Zhou (State Key Laboratory of Experimental Haematology in China) for this project. All core content of this thesis (including the abstract, introduction, methods, results, and discussion) was independently completed by the author team; no artificial intelligence (AI) software was used, and this work complies with the requirements of academic integrity.

Supporting Information

Additional supporting information can be found online in the Supporting Information section. (*Supporting Information*) Figure S1: The iPSC reprograming process with morphology changes at different stages from primary VSMC to established iPSC colonies. Scale bar = 250 μm. Figure S2: The cell morphology changes during mesoderm-mediated SMC differentiation from iPSCs. Scale bar = 250 μm.

References

[1] A. Evangelista, E. M. Iisselbacher, E. Bossone, et al., "Insights From the International Registry of Acute Aortic Dissection: A. 20-Year Experience of Collaborative Clinical Research," *Circulation* 137, no. 17 (2018): 1846–1860.

[2] C. A. Nienaber, R. E. Clough, N. Sakalihasan, et al., "Aortic Dissection," *Nature Reviews Disease Primers* 2, no. 1 (2016): 16053.

[3] B. Rylski, O. Schilling, and M. Czerny, "Acute Aortic Dissection: Evidence, Uncertainties, and Future Therapies," *European Heart Journal* 44, no. 10 (2023): 813–821.

[4] S. A. LeMaire and L. Russell, "Epidemiology of Thoracic Aortic Dissection," *Nature Reviews Cardiology* 8, no. 2 (2011): 103–113.

[5] A. Pinard, G. T. Jones, and D. M. Milewicz, "Genetics of Thoracic and Abdominal Aortic Diseases," *Circulation Research* 124, no. 4 (2019): 588–606.

[6] T. Faggion Vinholo, A. J. Brownstein, B. A. Ziganshin, et al., "Genes Associated With Thoracic Aortic Aneurysm and Dissection: 2019 Update and Clinical Implications," *AORTA* 07, no. 4 (2019): 99–107.

[7] T. Carrel, T. M. Sundt 3rd, Y. Von Kodolitsch, and M. Czerny, "Acute Aortic Dissection," *Lancet* 10378 (2023): 773–788.

[8] D. Wu, Y. H. Shen, L. Russell, J. S. Coselli, and S. A. LeMaire, "Molecular Mechanisms of Thoracic Aortic Dissection," *The Journal of Surgical Research* 184, no. 2 (2013): 907–924.

[9] L. B. Smith, P. W. F. Hadoke, E. Dyer, et al., "Haploinsufficiency of the Murine Col3a1 Locus Causes Aortic Dissection: A Novel Model of the Vascular Type of Ehlers–Danlos Syndrome," *Cardiovascular Research* 90, no. 1 (2011): 182–190.

[10] O. Rahkonen, M. Su, H. Hakovirta, et al., "Mice With a Deletion in the First Intron of the Col1a1 Gene Develop Age-Dependent Aortic Dissection and Rupture," *Circulation Research* 94, no. 1 (2004): 83–90.

[11] B. T. Weis-Müller, O. Modlich, I. Drobinskaya, et al., "Gene Expression in Acute Stanford Type A Dissection: A Comparative Microarray Study," *Journal of Translational Medicine* 4, no. 1 (2006): 29.

[12] J.-B. Michel, G. Jondeau, and D. M. Milewicz, "From Genetics to Response to Injury: Vascular Smooth Muscle Cells in Aneurysms and Dissections of the Ascending Aorta," *Cardiovascular Research* 114, no. 4 (2018): 578–589.

[13] K. Ren, B. Li, Z. Liu, et al., "GDF11 Prevents the Formation of Thoracic Aortic Dissection in Mice: Promotion of Contractile Transition of Aortic SMCs," *Journal of Cellular and Molecular Medicine* 25, no. 10 (2021): 4623–4636.

[14] G. Ailawadi, C. W. Moehle, H. Pei, et al., "Smooth Muscle Phenotypic Modulation is an Early Event in Aortic Aneurysms," *The Journal of Thoracic and Cardiovascular Surgery* 138, no. 6 (2009): 1392–1399.

[15] A. A. Singh, D. K. Shetty, A. G. Jacob, S. Bayraktar, and S. Sinha, "Understanding Genomic Medicine for Thoracic Aortic Disease through the Lens of Induced Pluripotent Stem Cells," *Frontiers in Cardiovascular Medicine* 11 (2024): 1349548.

[16] K. Musunuru, F. Sheikh, R. M. Gupta, et al., "Induced Pluripotent Stem Cells for Cardiovascular Disease Modeling and Precision Medicine: A Scientific Statement From the American Heart Association," *Circulation: Genomic and Precision Medicine* 11, no. 1 (2018): e000043.

[17] D. T. Paik, M. Chandy, and J. C. Wu, "Patient and Disease-Specific Induced Pluripotent Stem Cells for Discovery of Personalized Cardiovascular Drugs and Therapeutics," *Pharmacological Reviews* 72, no. 1 (2020): 320–342.

[18] A. Granata, F. Serrano, W. G. Bernard, et al., "An iPSC-Derived Vascular Model of Marfan Syndrome Identifies Key Mediators of Smooth Muscle Cell Death," *Nature Genetics* 49, no. 1 (2017): 97–109.

[19] P. Jin, S. Wang, X. Jiang, et al., "Generation of Human Induced Pluripotent Stem Cell Line (WMUi001-A) From a Patient With Aortic Dissection," *Stem Cell Research* 43 (2020): 101730.

[20] L. V. Rodriguez, Z. Alfonso, R. Zhang, et al., "Clonogenic Multipotent Stem Cells in Human Adipose Tissue Differentiate into Functional Smooth Muscle Cells," *Proceedings of the National Academy of Sciences of the United States of America* 103, no. 32 (2006): 12167–12172.

[21] C. Kime, T. A. Rand, K. N. Ivey, D. Srivastava, S. Yamanaka, and K. Tomoda, "Practical Integration-Free Episomal Methods for Generating Human Induced Pluripotent Stem Cells," *Current Protocols in Human Genetics* 87 (2015), 21.2.

[22] M. C. Galmiche, V. E. Koteliansky, J. Briere, P. Herve, and P. Charbord, "Stromal Cells From Human Long-Term Marrow Cultures Are Mesenchymal Cells that Differentiate following a Vascular Smooth Muscle Differentiation Pathway," *Blood* 82, no. 1 (1993): 66–76.

[23] Z. Wang, Y. Quan, M. Hu, et al., "VGLL4-TEAD1 Promotes Vascular Smooth Muscle Cell Differentiation From Human Pluripotent Stem Cells via TET2," *Journal of Molecular and Cellular Cardiology* 176 (2023): 21–32.

[24] D. M. Milewicz, K. M. Trybus, D.-C. Guo, et al., "Altered Smooth Muscle Cell Force Generation as a Driver of Thoracic Aortic Aneurysms and Dissections," *Arteriosclerosis, Thrombosis, and Vascular Biology* 37, no. 1 (2017): 26–34.

[25] A. Chakraborty, Y. Li, C. Zhang, et al., "Epigenetic Induction of Smooth Muscle Cell Phenotypic Alterations in Aortic Aneurysms and Dissections," *Circulation* 148, no. 12 (2023): 959–977.

[26] D. S. Kuo, C. Labelle-Dumais, and D. B. Gould, "COL4A1 and COL4A2 Mutations and Disease: Insights Into Pathogenic Mechanisms and Potential Therapeutic Targets," *Human Molecular Genetics* 21, no. R1 (2012): R97–R110.

[27] M. E. Meuwissen, D. J. Halley, L. S. Smit, et al., "The Expanding Phenotype of COL4A1 and COL4A2 Mutations: Clinical Data on 13 Newly Identified Families and a Review of the Literature," *Genetics in Medicine* 17, no. 11 (2015): 843–853.

[28] C. Liu, A. Oikonomopoulos, W. U. Sayed, and J. C Wu, "Modeling Human Diseases With Induced Pluripotent Stem Cells: From 2D to 3D and Beyond," *Development* 145, no. 5 (2018).

[29] I. Itzhaki, L. Maizels, I. Huber, et al., "Modelling the Long QT Syndrome With Induced Pluripotent Stem Cells," *Nature* 471, no. 7337 (2011): 225–229.

[30] C. Kim, J. Wong, J. Wen, et al., "Studying Arrhythmogenic Right Ventricular Dysplasia With Patient-Specific iPSCs," *Nature* 494, no. 7435 (2013): 105–110.

[31] L. de Figueiredo Borges, R. G. Jaldin, R. R. Dias, et al., "Collagen Is Reduced and Disrupted in Human Aneurysms and Dissections of Ascending Aorta," *Human Pathology* 39, no. 3 (2008): 437–443.

[32] Z. Li, C. Zhou, L. Tan, et al., "Variants of Genes Encoding Collagens and Matrix Metalloproteinase System Increased the Risk of Aortic Dissection," *Science China Life Sciences* 60, no. 1 (2017): 57–65.

[33] E. Plaisier, O. Gribouval, S. Alamowitch, et al., "COL4A1 Mutations and Hereditary Angiopathy, Nephropathy, Aneurysms, and Muscle Cramps," *The New England Journal of Medicine* 357, no. 26 (2007): 2687–2695.

[34] V. S. Lee, C. M. Halabi, E. P. Hoffman, et al., "Loss of Function Mutation in LOX Causes Thoracic Aortic Aneurysm and Dissection in Humans," *Proceedings of the National Academy of Sciences of the United States of America* 113, no. 31 (2016): 8759–8764.

[35] S. Inamoto, C. S. Kwartler, A. L. Lafont, et al., "TGFBR2 Mutations Alter Smooth Muscle Cell Phenotype and Predispose to Thoracic Aortic Aneurysms and Dissections," *Cardiovascular Research* 88, no. 3 (2010): 520–529.

[36] G. Zhao, Y. Fu, Z. Cai, et al., "Unspliced XBP1 Confers VSMC Homeostasis and Prevents Aortic Aneurysm Formation via FoxO4 Interaction," *Circulation Research* 121, no. 12 (2017): 1331–1345.

[37] L. X. Jia, W. M. Zhang, H. J. Zhang, et al., "Mechanical Stretch-Induced Endoplasmic Reticulum Stress, Apoptosis and Inflammation Contribute to Thoracic Aortic Aneurysm and Dissection," *The Journal of Pathology* 236, no. 3 (2015): 373–383.

[38] D. M. Milewicz and F. Ramirez, "Therapies for Thoracic Aortic Aneurysms and Acute Aortic Dissections," *Arteriosclerosis, Thrombosis, and Vascular Biology* 39, no. 2 (2019): 126–136.

[39] J. P. Habashi, D. P. Judge, T. M. Holm, et al., "Losartan, an AT1 Antagonist, Prevents Aortic Aneurysm in a Mouse Model of Marfan Syndrome," *Science* 312, no. 5770 (2006): 117–121.

[40] N. W. Ramnath, L. J. Hawinkels, P. M. Van Heihningen, et al., "Fibulin-4 Deficiency Increases TGF-β Signalling in Aortic Smooth Muscle Cells due to Elevated TGF-β2 Levels," *Scientific Reports* 5, no. 1 (2015): 16872.

[41] W. Li, Q. Li, Y. Jiao, et al., "Tgfbr2 Disruption in Postnatal Smooth Muscle Impairs Aortic Wall Homeostasis," *The Journal of Clinical Investigation* 124, no. 2 (2014): 755–767.

[42] H. Wei, J. H. Hu, S. N. Angelov, et al., "Aortopathy in a Mouse Model of Marfan Syndrome is Not Mediated by Altered Transforming Growth Factor Beta Signaling," *Journal of the American Heart Association* 6, no. 1 (2017).

[43] T. M. Holm, J. P. Habashi, J. J. Doyle, et al., "Noncanonical TGFbeta Signaling Contributes to Aortic Aneurysm Progression in Marfan Syndrome Mice," *Science* 332, no. 6027 (2011): 358–361.

[44] P. Jin, Y. Xu, S. Wang, et al., "Modeling Thoracic Aortic Dissection Using Patient-Specific iPSCs Reveals VSMC Dysfunction and Extracellular Matrix Dysregulation," *bioRxiv* (2024).